RESEARCH ARTICLE SUMMARY

IMMUNOMETABOLISM

Tumor necrosis factor induces pathogenic mitochondrial ROS in tuberculosis through reverse electron transport

Francisco J. Roca, Laura J. Whitworth, Hiran A. Prag, Michael P. Murphy, Lalita Ramakrishnan*

INTRODUCTION: Tumor necrosis factor (TNF) mediates resistance to tuberculosis. Excess TNF production, however, is detrimental because it induces pathogenic necrosis of infected macrophages in the tuberculous granuloma, which releases the mycobacteria into the extracellular milieu, promoting their growth and transmission to new hosts. Excess TNF, through the kinase RIP3 and the mitochondrial phosphatase PGAM5, increases reactive oxygen species such as superoxide and hydrogen peroxide in the mitochondria of mycobacterium-infected macrophages. These mitochondrial reactive oxygen species (mROS) initiate an elaborate interorganellar signaling circuit that ultimately causes macrophage necrosis and release of mycobacteria.

RATIONALE: How TNF signaling elevates mROS production is not known. To address this question in vivo, we used zebrafish larvae, taking advantage of their optical transparency and their amenability to genetic and pharmacological manipulation. Thus, we could visualize and quantify mROS and macrophage necrosis after these manipulations.

RESULTS: Typically, mROS are generated during normal respiration when electrons from reduced nicotinamide adenine dinucleotide (NADH), produced by metabolic pathways, enter the electron transport chain (ETC) and are transferred by forward electron transport from complex I to coenzyme Q (CoQ). We found that in wild-type animals without excess TNF, mycobacterial infection induced a small boost in multiple metabolic pathways that increased mROS through this process. This slight increase in mROS did not result in macrophage necrosis. In animals with excess TNF (TNF^{hi} animals), we found that the greatly increased mROS were not induced through conventional forward electron transport but rather through reverse electron transport (RET). RET occurs when increases in the pool of reduced CoQ ($CoQH_2$) from various metabolic pathways—in conjunction with a high proton-motive force across the mitochondrial inner membrane—cause electrons to flow back through complex I instead of forward into complex III. RET can generate large amounts of mROS at complex I. We found that increased oxidation of succinate at complex II was responsible for RET mROS and that this metabolite was the source of the accumulation of $CoQH_2$. Succinate is produced in the Krebs cycle, so we investigated its metabolic source. We found that TNF increased glutamine transport into the cell, boosting glutaminolysis, which increases the pool of α-ketoglutarate supplied to the Krebs cycle, resulting in increased succinate.

Mycobacteria play a critical role in TNF-induced necrosis at two distinct steps. They were required together with TNF to increase glutaminolysis and then again with the resultant mROS to induce necrosis. By contrast, TNF had no further role in the necrosis pathway beyond inducing mROS. Thus, virulent mycobacteria have evolved multiple orchestrated mechanisms to exploit host genetic vulnerabilities (i.e., dysregulated TNF levels) to mediate macrophage necrosis as a way of increasing the transmission that is critical to their survival. Delineation of the TNF-induced RET mROS pathway identified several drugs, already approved for other conditions, that inhibit the pathway at different steps. These drugs also inhibited TNF-induced macrophage necrosis and the animals' hypersusceptibility to infection.

CONCLUSION: RET, long thought to be an in vitro artifact, is now appreciated to play important homeostatic roles through moderate increases in mROS. However, excess RET has been shown to mediate the pathology associated with ischemia-reperfusion injury in heart attack and stroke. Our work shows that RET mROS also mediates tuberculosis pathology. Paradoxically, this means that the critical host determinant TNF can go from being protective to pathogenic depending on relative concentration, context, and the extent to which it can modulate host metabolism. Our prior work has shown that dysregulated TNF is also pathogenic in human tuberculosis. Therefore, the pathway-inhibiting drugs we have identified are promising host-targeting adjunctive drugs for tuberculosis, both drug-sensitive and drug-resistant. Metformin—a widely used, well-tolerated antidiabetic drug as well as a complex I inhibitor—is a particularly good candidate. ■

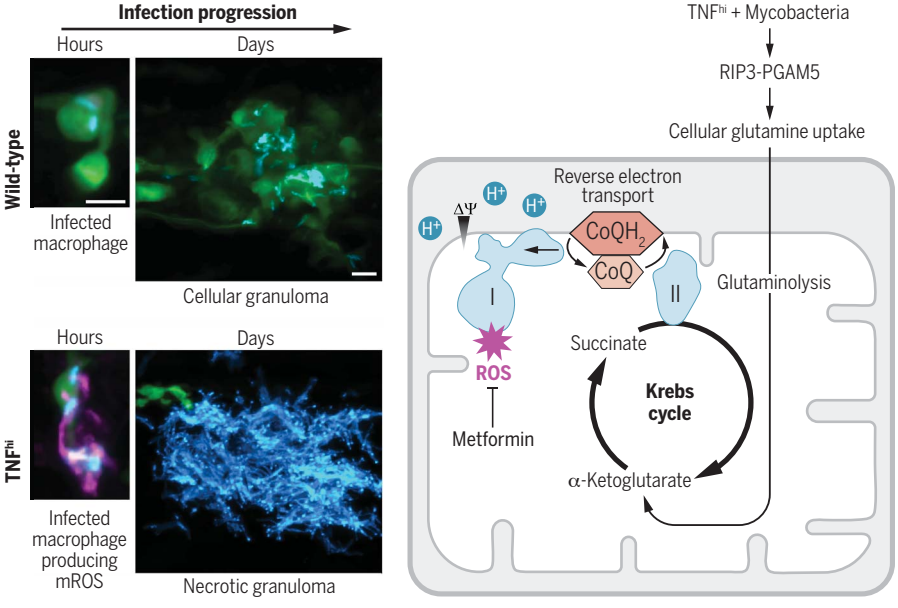

Excess TNF induces pathological mROS via RET in tuberculosis. Left: TNF induces mROS (magenta) in macrophages (green) infected with mycobacteria (blue), which causes their necrosis with exuberant growth of released mycobacteria in the debris of the tuberculosis granuloma. Right: Schematic depiction of how TNF works through RIP3 and PGAM5 to elevate mROS by RET through complex I. Metformin inhibits complex I to prevent TNF-induced mROS.

The list of author affiliations is available in the full article online.
*Corresponding author. Email: lalitar@mrc-lmb.cam.ac.uk
Cite this article as F. J. Roca *et al.*, *Science* **376**, eabh2841 (2022). DOI: 10.1126/science.abh2841

READ THE FULL ARTICLE AT
https://doi.org/10.1126/science.abh2841

Downloaded from https://www.science.org at University Van Amsterdam on April 13, 2025

RESEARCH ARTICLE

IMMUNOMETABOLISM

Tumor necrosis factor induces pathogenic mitochondrial ROS in tuberculosis through reverse electron transport

Francisco J. Roca[1]†, Laura J. Whitworth[1,2], Hiran A. Prag[3], Michael P. Murphy[1,3], Lalita Ramakrishnan[1,2]*

Tumor necrosis factor (TNF) is a critical host resistance factor against tuberculosis. However, excess TNF produces susceptibility by increasing mitochondrial reactive oxygen species (mROS), which initiate a signaling cascade to cause pathogenic necrosis of mycobacterium-infected macrophages. In zebrafish, we identified the mechanism of TNF-induced mROS in tuberculosis. Excess TNF in mycobacterium-infected macrophages elevates mROS production by reverse electron transport (RET) through complex I. TNF-activated cellular glutamine uptake leads to an increased concentration of succinate, a Krebs cycle intermediate. Oxidation of this elevated succinate by complex II drives RET, thereby generating the mROS superoxide at complex I. The complex I inhibitor metformin, a widely used antidiabetic drug, prevents TNF-induced mROS and necrosis of *Mycobacterium tuberculosis*–infected zebrafish and human macrophages; metformin may therefore be useful in tuberculosis therapy.

Tumor necrosis factor (TNF) is both a host resistance and susceptibility factor in tuberculosis (TB) (*1*–*3*). Findings in the genetically tractable and optically transparent zebrafish larva infected with *Mycobacterium marinum* (*Mm*) have revealed the mechanisms behind this dual effect (*4*–*6*). Although TNF is required for full microbicidal activity of mycobacterium-infected macrophages, its excess causes susceptibility by inducing their necrotic death, which releases mycobacteria into the growth-permissive extracellular environment (*4*, *7*–*9*). This pathogenic role of dysregulated TNF was revealed through a zebrafish forward genetic screen, which found that both a deficiency and an excess of leukotriene A4 hydrolase (LTA4H) cause susceptibility to *Mm* (*4*, *9*). LTA4H catalyzes the synthesis of the proinflammatory leukotriene B4 (LTB_4), and LTA4H/LTB_4 deficiency and excess produce TNF deficiency and excess, respectively (*4*). These zebrafish studies led to the identification of a common, functional human *LTA4H* variant associated with mortality from tuberculous meningitis, the severest form of TB (*4*, *10*). In cohorts in Vietnam and Indonesia, the high LTA4H–expressing variant was associated with increased cerebrospinal fluid TNF levels and increased mortality that was mitigated by adjunctive treatment with corticosteroids, broadly acting immunosuppressants (*3*, *4*, *10*). These findings implicated LTB_4 and TNF-induced inflammation in mortality (*3*, *4*, *10*). Moreover, high TNF concentrations were associated with mortality even among individuals without the high LTA4H–expressing variant; this suggested that TNF excess, resulting from diverse host genetic determinants, is a far-reaching host susceptibility factor in TB (*3*). Consistent with these findings, necrotic human tuberculous granulomas have more TNF than non-necrotic ones (*11*).

To gain mechanistic understanding of TNF-mediated pathogenic macrophage necrosis, we returned to the zebrafish larva. We found that excess TNF, acting through the kinase RIP3 and one of its substrates, PGAM5, increases mitochondrial reactive oxygen species (mROS) such as superoxide and hydrogen peroxide in infected macrophages (fig. S1) (*5*, *6*). These mROS activate an interorganellar signaling circuit that involves the lysosome and the endoplasmic reticulum. This ultimately causes mitochondrial calcium overload, which then leads to necrosis (fig. S1) (*5*, *6*). By exploiting the zebrafish larva's genetic and pharmacological tractability, we were able to determine how TNF induces pathogenic mROS in mycobacterium-infected macrophages.

TNF induces mROS through RET

Administering exogenous TNF to *Mm*-infected zebrafish larvae phenocopies genetically induced TNF excess, causing macrophage necrosis and susceptibility by 5 days after infection (fig. S2) (*4*). TNF selectively induces mROS in infected macrophages within 30 min, which rapidly triggers necrosis (*5*, *6*). Using a general mitochondria-targeted ROS and oxidative stress sensor, we found that in wild-type animals, *Mm* infection alone causes increases in mROS in infected macrophages by a factor of 1.7 to 2.2 relative to uninfected macrophages in the same animal (Fig. 1, A and B). In TNF^{hi} animals, mROS in infected macrophages were further increased by a factor of 3.6 to 6.6 relative to uninfected macrophages (Fig. 1, A and B). TNF did not increase mROS in uninfected macrophages, hence only infected macrophages were susceptible to TNF's effects (Fig. 1, A and B). Moreover, heat-killed *Mm* failed to induce mROS in both wild-type and TNF^{hi} animals, which suggested that an actively synthesized (or heat-labile) bacterial determinant is needed (Fig. 1B). To confirm that the increased TNF^{hi} mROS originated from superoxide production by the electron transport chain (ETC), we asked whether it was inhibited by compounds that disrupt mitochondrial electron transport. mROS were inhibited by four compounds that disrupt mitochondrial electron transport through distinct mechanisms (Fig. 1, C to F, fig. S2, and table S1). Thus, TNF-induced mROS originate in the ETC of mycobacterium-infected macrophages.

During normal respiration, complex I receives electrons from NADH (reduced nicotinamide adenine dinucleotide) and transfers them to CoQ (coenzyme Q), generating in the process a small amount of the mROS superoxide ($O_2^{\bullet-}$) through single electron donation to O_2 (*12*) (Fig. 2A). Increased $O_2^{\bullet-}$ production at complex I is generated by two distinct mechanisms (*12*). In the first, disruption of electron transfer, due to ETC damage or loss of cytochrome C during apoptosis, results in an accumulation of NADH derived from multiple metabolic pathways. When electrons from NADH enter complex I and cannot flow forward toward ubiquinone, they generate $O_2^{\bullet-}$ (Fig. 2A). In the second mechanism, increases in the extent of CoQ pool reduction ($CoQH_2$) from various metabolic pathways, in conjunction with a high proton-motive force across the mitochondrial inner membrane, cause electrons to flow back through complex I instead of forward into complex III (Fig. 2B) (*13*). This reverse electron transport (RET) by complex I generates mROS ($O_2^{\bullet-}$, which dismutates to H_2O_2) (Fig. 2B). These two mechanisms can be distinguished by the effects of the complex I inhibitor rotenone, which increases mROS from forward electron flow through complex I but reduces mROS from RET (Fig. 2, A and B, and table S1) (*12*, *14*). Rotenone increased mROS in the infected macrophages of wild-type animals, showing that they were generated by forward electron transport (Fig. 2C). By contrast, rotenone inhibited mROS in TNF^{hi} animals (Fig. 2D). Two other complex I inhibitors with different mechanisms of action also

[1]Molecular Immunity Unit, Cambridge Institute of Therapeutic Immunology and Infectious Diseases, Department of Medicine, University of Cambridge, Cambridge CB2 0AW, UK. [2]MRC Laboratory of Molecular Biology, Cambridge CB2 0QH, UK. [3]MRC Mitochondrial Biology Unit, University of Cambridge, Cambridge CB2 0XY, UK.
*Corresponding author. Email: lalitar@mrc-lmb.cam.ac.uk
†Present address: Department of Biochemistry and Molecular Biology–B and Immunology, Biomedical Research Institute of Murcia (IMIB-Arrixaca), University of Murcia, 30120 Murcia, Spain.

Downloaded from https://www.science.org at University Van Amsterdam on April 13, 2025

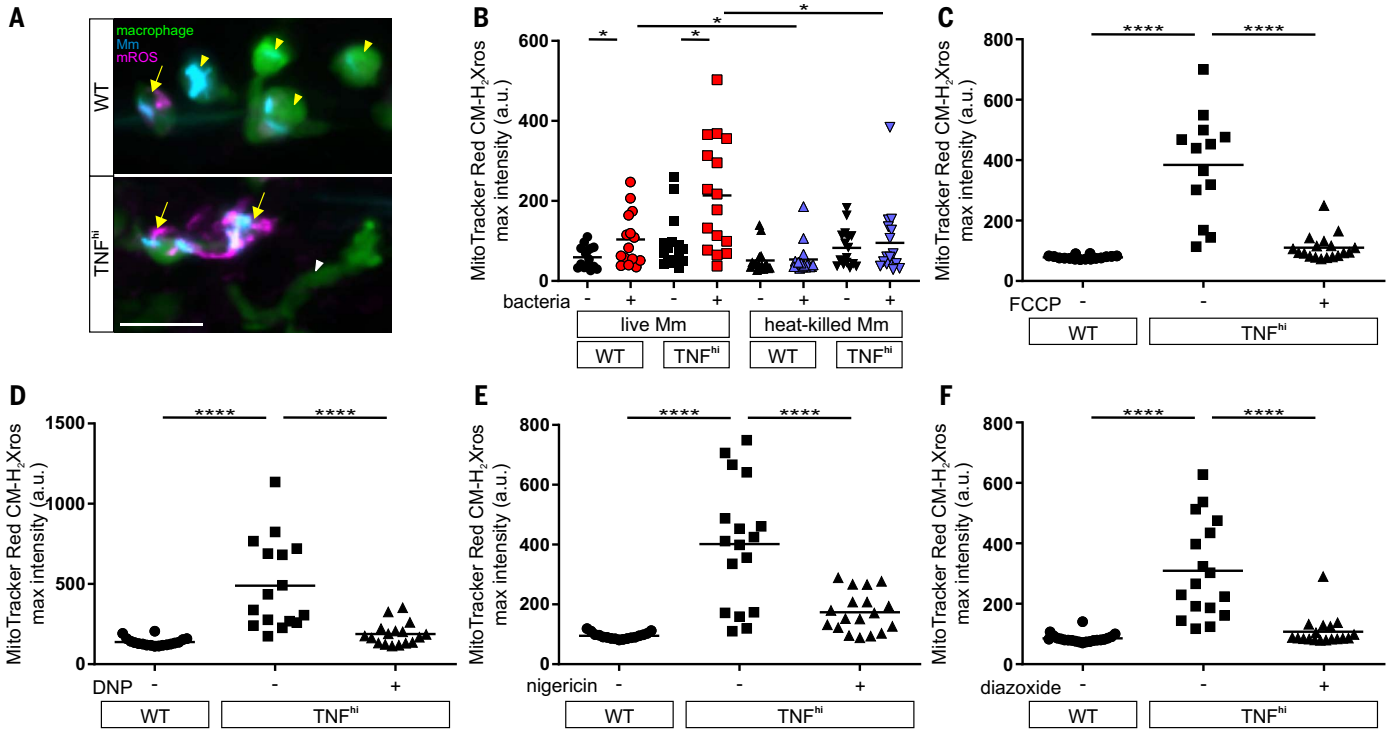

Fig. 1. ETC-derived mROS drive necrosis of *Mm*-infected macrophages in TNF-high conditions. (**A**) Representative pseudocolored confocal images of wild-type or TNF^{hi} larvae with yellow fluorescent protein (YFP)–expressing macrophages (green), 1 day after infection with EBFP2-expresssing *Mm* (blue), showing MitoTracker Red CM-H_2Xros (magenta) fluorescence. White arrowheads, uninfected macrophages; yellow arrowheads, infected macrophages; yellow arrows, infected macrophages positive for mROS. Scale bar, 20 μm. (**B**) Quantification of mROS in wild-type or TNF^{hi} larvae 9 hours after injection of live or heat-killed *Mm*. Each point represents the mean maximum intensity fluorescence of MitoTracker Red CM-H_2Xros per fish. Black symbols represent macrophages that do not contain bacteria. Red and purple symbols represent *Mm*-infected and heat-killed *Mm*-containing macrophages, respectively, in the same animal. Horizontal bars denote means; *P < 0.05 (one-way ANOVA with uncorrected Dunn's post-test for differences between macrophages in the same animal and with Tukey's post-test for differences between treatments). Data are representative of two independent experiments. (**C** to **F**) Quantification of mROS in larvae 1 day after infection with *Mm* that are wild-type or TNF^{hi} treated with FCCP (C), DNP (D), nigericin (E), or diazoxide (F), or vehicle. Horizontal bars denote means; ****P < 0.0001 (one-way ANOVA with Tukey's post-test). Data are representative of two or three independent experiments.

inhibited TNF^{hi} mROS (fig. S3 and table S1). Thus, TNF^{hi} mROS are generated by RET rather than by forward electron transport.

To corroborate that RET was responsible for TNF^{hi} mROS, we expressed *Ciona intestinalis* alternative oxidase (AOX) in TNF^{hi} larvae through injection of its mRNA. AOXs, which are present in plants, fungi, and some invertebrates but are absent in vertebrates, catalyze the transfer of electrons from the $CoQH_2$ pool directly to O_2, bypassing complexes III and IV (fig. S4A) (*15*). AOX has been shown to prevent excessive reduction of the CoQ pool and mROS increases from RET (fig. S4A) (*15*). Thus, if TNF-induced mROS are generated by RET, they should be prevented by AOX expression (*15*). We confirmed that the *C. intestinalis* AOX was active in zebrafish by showing that AOX-expressing animals were resistant to cyanide, which poisons the ETC by inhibiting complex IV (fig. S4B) (*15*, *16*). AOX expression decreased TNF^{hi} mROS, consistent with generation by RET from a reduced CoQ pool (Fig. 2, B and E).

Finally, we extended these findings to *M. tuberculosis* (*Mtb*), the agent of human TB, using a leucine and pantothenic acid *Mtb* auxotroph that can be used in containment level 2 facilities (*6*). *Mtb* produced increases in mROS similar to those produced by *Mm* (Fig. 2F). Moreover, rotenone increased mROS in wild-type macrophages and inhibited TNF-induced mROS (Fig. 2, G and H). Thus, TNF-induced mROS increases in *Mtb*-infected macrophages are also derived from RET.

Although there are multiple sources of increased $CoQH_2$, the most compelling candidate from both in vitro and in vivo studies was the increased oxidation of succinate at complex II (Fig. 2B) (*13*, *17*). We tested this idea using three complex II inhibitors: atpenin A, thenoyltrifluoroacetone (TTFA), and dimethyl malonate (DM-malonate), which is a prodrug of the competitive succinate dehydrogenase inhibitor malonate. All three inhibitors abolished mROS (Fig. 3A and table S1). If increased succinate oxidation at complex II were the source of RET and mROS, then increasing the mitochondrial succinate pool should have induced mROS even in wild-type animals in the absence of TNF^{hi} conditions. Diethyl succinate—a cell-permeable succinate ester known to increase mitochondrial succinate concentrations (*18*)—increased mROS in macrophages of wild-type animals (Fig. 3B). Diethyl butylmalonate (DEBM)—an inhibitor of the mitochondrial succinate transporter, which causes accumulation of endogenous mitochondrial succinate (*19*)—performed similarly (Fig. 3B). Thus, increased oxidation of succinate at complex II is necessary and sufficient for TNF-induced RET and mROS.

TNF-activated glutaminolysis increases mitochondrial succinate

We next investigated the metabolic source of the increased succinate concentration. Increased glycolysis, fatty acid oxidation, and glutaminolysis can all increase succinate by increasing Krebs cycle activity through increased input of pyruvate, acetyl-CoA, and α-ketoglutarate, respectively (Fig. 4A). We

Downloaded from https://www.science.org at University Van Amsterdam on April 13, 2025

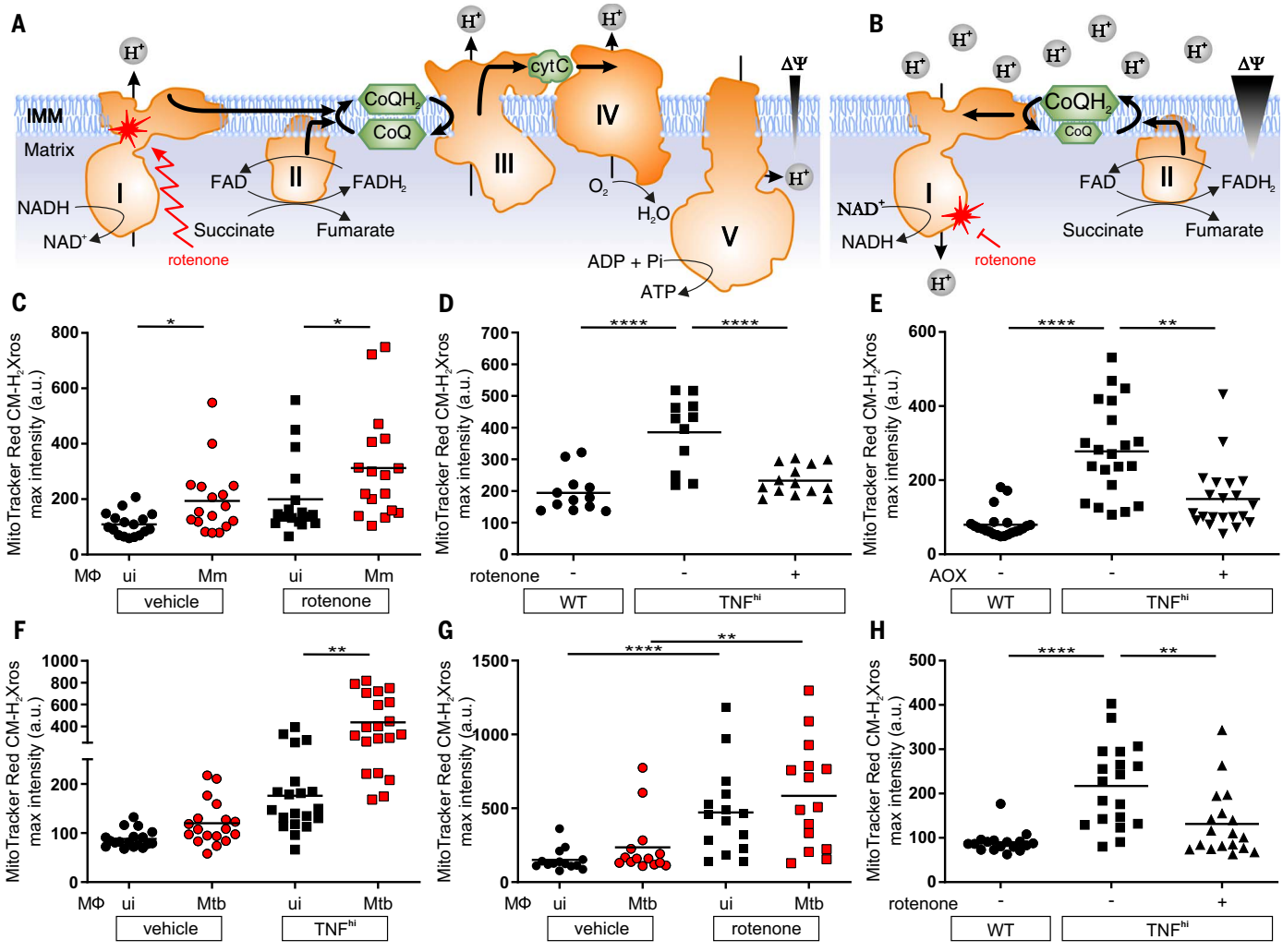

Fig. 2. TNF induces RET mROS at complex I in mycobacterium-infected macrophages. (**A** and **B**) Illustrations of mROS production at complex I during forward electron transport (A) and reverse electron transport (B). FAD, flavin adenine dinucleotide; ΔΨ, membrane potential; IMM, inner mitochondrial membrane; ADP/ATP, adenosine diphosphate/triphosphate; cytC, cytochrome C; I to V, complexes I to V; zigzag arrows, induction; red blunted arrows, inhibition. (**C** to **H**) Quantification of mROS in larvae 1 day after infection with *Mm* [(C) to (E)] or *Mtb* [(F) to (H)] that are wild-type treated with rotenone or vehicle (C); wild-type or TNF^{hi} treated with rotenone or vehicle (D); wild-type, TNF^{hi}, or TNF^{hi} expressing AOX (E); wild-type or TNF^{hi} (F); wild-type treated with rotenone or vehicle (G); or wild-type or TNF^{hi} treated with rotenone or vehicle (H). Horizontal bars denote means; $^{*}P < 0.05$, $^{**}P < 0.01$, $^{****}P < 0.0001$ [one-way ANOVA with Dunn's post-test in (C), (G), and (H); Tukey's post-test in (D) and (E); uncorrected Dunn's post-test in (F)]. Black and red symbols in (C), (F), and (G) represent uninfected (ui) and infected macrophages, respectively, in the same animals. Data are representative of two or three independent experiments [(C to G)] or a single experiment (H).

Downloaded from https://www.science.org at University Van Amsterdam on April 13, 2025

Fig. 3. TNF increases succinate-dependent mROS in mycobacterium-infected macrophages. (**A** and **B**) Quantification of mROS in larvae 1 day after infection with *Mm* that are wild-type or TNF^{hi} treated with atpenin A, TTFA, DM-malonate, or vehicle (A) or wild-type treated with succinate, DEBM, or vehicle. Horizontal bars denote means; $^{*}P < 0.05$, $^{**}P < 0.01$, $^{***}P < 0.001$,$^{****}P < 0.0001$ [one-way ANOVA with Tukey's post-test (A) or Dunn's post-test (B)]. Black and red symbols in (B) represent uninfected (ui) and *Mm*-infected (*Mm*) macrophages, respectively, in the same animal. Data are representative of two or three independent experiments.

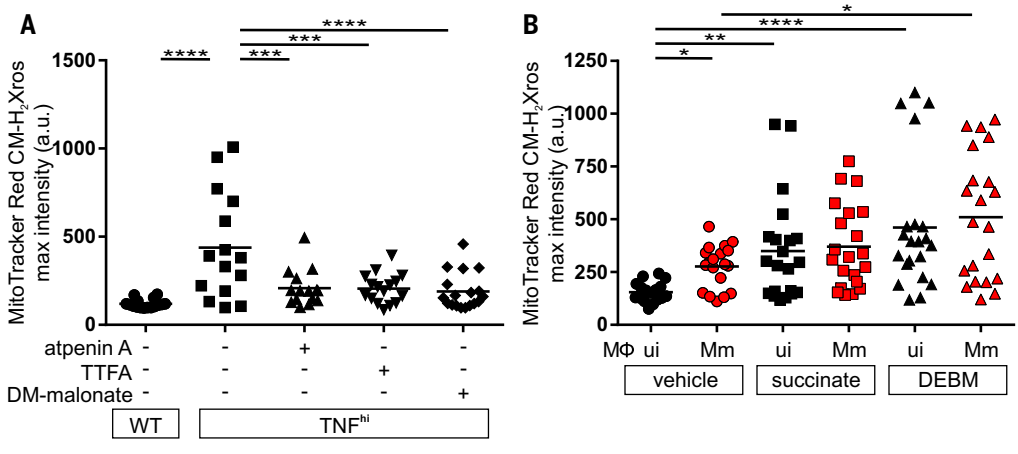

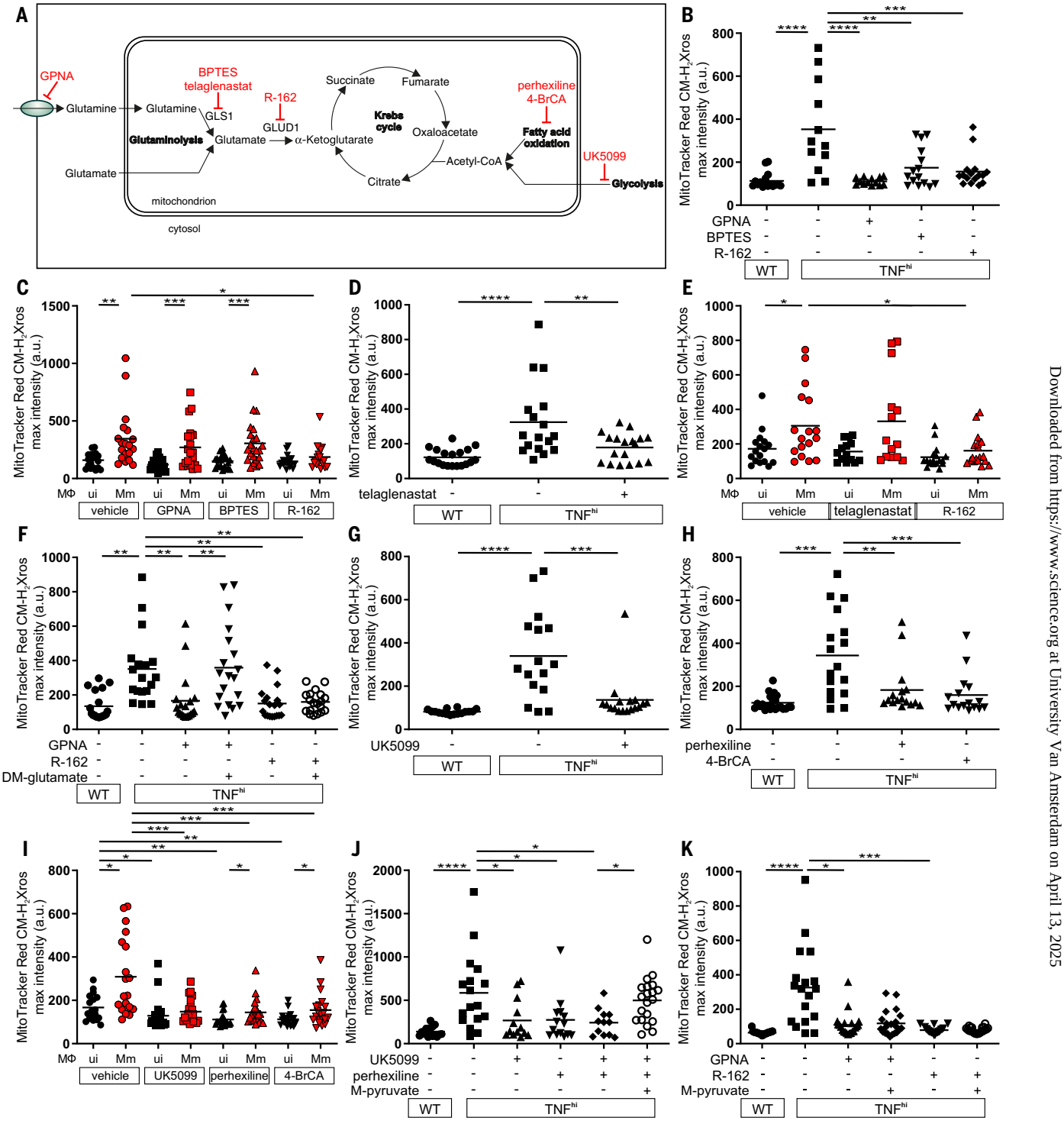

Fig. 4. TNF-induced glutamine cellular uptake and increased glutaminolysis is responsible for RET and mROS production in mycobacterium-infected macrophages. (**A**) Illustration of main metabolic pathways fueling the Krebs cycle with inhibitors used (truncated red arrows). GLUD1, glutamate dehydrogenase 1. (**B** to **K**) Quantification of mROS in larvae 1 day after infection with *Mm* that are wild-type or TNF^{hi} treated with GPNA, BPTES, R-162, or vehicle (B); wild-type treated with GPNA, BPTES, R-162, or vehicle (C); wild-type or TNF^{hi} treated with telaglenastat or vehicle (D); wild-type treated with telaglenastat, R-162, or vehicle (E); wild-type or TNF^{hi} treated with vehicle, or GPNA or R-162 alone or in combination with DM-glutamate (F); wild-type or TNF^{hi} treated with UK5099 or vehicle (G); wild-type or TNF^{hi} treated with perhexiline, 4-BrCA, or vehicle (H); wild-type treated with UK5099, perhexiline, 4-BrCA, or vehicle (I); wild-type or TNF^{hi} treated with vehicle, or UK5099 or perhexiline alone or in combination with M-pyruvate (J); or GPNA or R-162 alone or in combination with M-pyruvate (K). Horizontal bars denote means; *P < 0.05, **P < 0.01, ***P < 0.001, ****P < 0.0001 [one-way ANOVA with Tukey's post-test in (B), (D), (F) to (H), (J), and (K); Dunn's post-test in (C), (E), and (I)]. Black and red symbols in (C), (E), and (I) represent uninfected (ui) and *Mm*-infected (*Mm*) macrophages, respectively, in the same animals. Data are representative of two or three independent experiments [(B) to (D), (G) to (I)] or a single experiment [(E), (F), (J), and (K)].

Downloaded from https://www.science.org at University Van Amsterdam on April 13, 2025

focused on glutaminolysis, which has been linked to TNF-mediated cell death (*20*, *21*). Glutamine, the major amino acid transported in the circulation, is taken up into cells by multiple glutamine transporters and then into mitochondria, where it is converted to glutamate and then α-ketoglutarate in the Krebs cycle (Fig. 4A). Four potential plasma membrane transporters that contribute to cellular glutamine uptake are highly expressed in human and zebrafish monocytes and macrophages (*22*–*24*). Of these, SLCA15 and SLC38A2 were identified in a screen for proteins phosphorylated by the RIP3 kinase in the context of necroptosis, a different form of TNF-mediated programmed cell death (*25*). Although distinct from necroptosis, our macrophage necrosis pathway also features RIP3, which is required for TNF-mediated mROS induction in mycobacterium-infected macrophages (fig. S1) (*5*, *6*). Therefore, we tested L-γ-glutamyl-p-nitroanilide (GPNA), an inhibitor of both transporters (table S1). GPNA inhibited mROS in TNF^{hi} macrophages without affecting mROS in wild-type macrophages (Fig. 4, A to C). We therefore hypothesized that TNF-RIP3–activated glutamine transport is the specific source of the increased mitochondrial glutamine for increased glutaminolysis, thereby increasing succinate. If correct, blocking the conversion of glutamine to glutamate should also specifically block TNF^{hi} mROS. Bis-2-(5-phenylacetamido-1,3,4-thiadiazol-2-yl)ethyl sulfide (BPTES) and CB-839 (telaglenastat), two different inhibitors of glutaminase 1 (GLS1), performed as expected, inhibiting mROS in TNF^{hi} but not wild-type macrophages (Fig. 4, A to E, and table S1). By contrast, when the conversion of glutamate to α-ketoglutarate was inhibited using R-162, mROS was inhibited in both TNF^{hi} and wild-type macrophages (Fig. 4, A, B, C, and E, and table S1). Thus, although the smaller increase in mROS from infection alone also requires glutaminolysis, it can be sustained by mitochondrial glutamate transported directly from the cytosol where it is produced through transamination reactions (Fig. 4A, C and E). Finally, to confirm the specificity of GPNA and R-162 in our system, we used each inhibitor in combination with dimethyl glutamate (DM-glutamate), a cell-permeable source of glutamate (table S1). Dimethyl glutamate restored GPNA-inhibited mROS but not R-162–inhibited mROS (Fig. 4F). Thus, TNF stimulation of infected macrophages specifically activates glutamine uptake to increase glutaminolysis to induce mROS.

If high TNF also increases glycolysis and/or fatty acid oxidation (Fig. 4A), then inhibiting these pathways should also specifically inhibit TNF^{hi} but not wild-type mROS. However, inhibition of mitochondrial pyruvate transport using UK5099 removed mROS in both wild-type and TNF^{hi} animals, as did inhibition of fatty acid oxidation using perhexiline or 4-bromocrotonic acid (4-BrCA) (Fig. 4, G to I, and table S1). We confirmed the specificity of UK5099 and perhexiline by showing that methyl pyruvate (M-pyruvate), a cell-permeable pyruvate derivative, restored mROS inhibited by them but not by GPNA or R-162 (Fig. 4, J and K, and table S1). Thus, TNF and infection together activate cellular glutamine uptake, and the resultant increase in glutaminolysis is the specific source of the increased succinate. Because oxidation of excess succinate would increase the concentrations of the downstream intermediates malate and oxaloacetate (a potent complex II inhibitor) (*26*), glycolysis and fatty acid oxidation would be required to play a "supporting role" by providing acetyl-CoA to consume oxaloacetate. Thus, the build-up of oxaloacetate would be prevented, allowing continued complex II activity (Fig. 4A).

We used liquid chromatography–mass spectrometry to quantify succinate concentrations in the larvae under the different conditions. Infection and TNF combined (but neither alone) increased succinate concentrations over baseline (Fig. 5A and data S1). Moreover, GPNA and BPTES inhibited this increase, as predicted (Fig. 5A and data S1). Although further validation of the source of succinate by measurement of flux to it from stable isotope–labeled precursors such as glutamine was not technically possible in this in vivo system, our findings that both mROS and succinate concentrations increase in the TNF^{hi} state and decrease to wild-type levels upon inhibiting glutamine uptake or its conversion to glutamate provide strong evidence that glutaminolysis from increased glutamine transport is the source of the increased succinate. As with mROS increases, these succinate increases also occurred rapidly within 30 min of TNF administration. The rapid induction of succinate and mROS is consistent with TNF-RIP3–induced posttranslational modifications (e.g., phosphorylation), as previously proposed (*20*, *21*). Accordingly, RIP3 knockdown inhibited TNF-induced succinate in infected animals (Fig. 5B and data S1). Finally, TNF-induced succinate was also inhibited by knockdown of PGAM5, a mitochondrial phosphatase, which is required together with RIP3 both for TNF-mediated necroptosis (*27*) and for TNF-induced mROS and necrosis of mycobacterium-infected macrophages in our pathway (Fig. 5B, data S1, and fig. S1) (*5*, *6*). Thus, TNF signals via RIP3 and PGAM5 to activate glutamine transport to increase glutaminolysis and Krebs cycle succinate.

TNF, mROS, and mycobacteria play discrete roles in macrophage necrosis

We dissected the interactions among TNF, mROS, and mycobacteria and their roles at distinct steps of the pathway. We had shown that both TNF and mycobacteria are required to increase mitochondrial succinate, which is required to induce mROS. Because exogenous succinate could induce mROS in wild-type animals in both infected and uninfected macrophages (Fig. 3B), we concluded that the only role for TNF and mycobacteria in mROS induction in this system is to increase mitochondrial succinate.

Downloaded from https://www.science.org at University Van Amsterdam on April 13, 2025

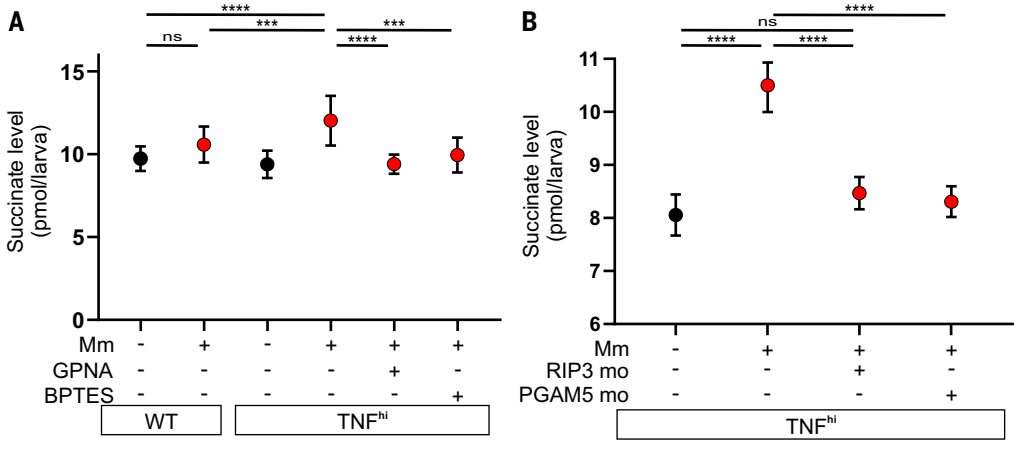

Fig. 5. TNF-induced glutaminolysis increases succinate levels in mycobacterium-infected macrophages in a RIP3- and PGAM5-dependent manner. (**A** and **B**) Quantification of succinate in zebrafish larvae 1 day after infection with *Mm* or mock-injected, that are wild-type or TNF^{hi} treated with GPNA, BPTES, or vehicle (A) and TNF^{hi}, TNF^{hi} RIP3 morphants, or TNF^{hi} PGAM5 morphants (B). Each point represents the mean of four independent experiments in (A) and two independent experiments in (B). Vertical bars denote pooled SD. ***$P < 0.001$, ****$P < 0.0001$ (one-way ANOVA with Tukey's post-test); ns, not significant.

We previously showed that mROS are required for macrophage necrosis (*5*). We now asked whether they were sufficient to complete macrophage necrosis, or whether TNF and/or mycobacteria were further required downstream of mROS induction. Macrophage necrosis results in exuberant extracellular mycobacterial growth in characteristic cords (Fig. 6A). Bacterial cording can be used as a reliable surrogate marker for infected macrophage death (*9*). We found that both exogenous succinate and DEBM induced the necrosis of infected macrophages, as evidenced by increased bacterial cording (Fig. 6B). This necrosis was a direct consequence of RET mROS

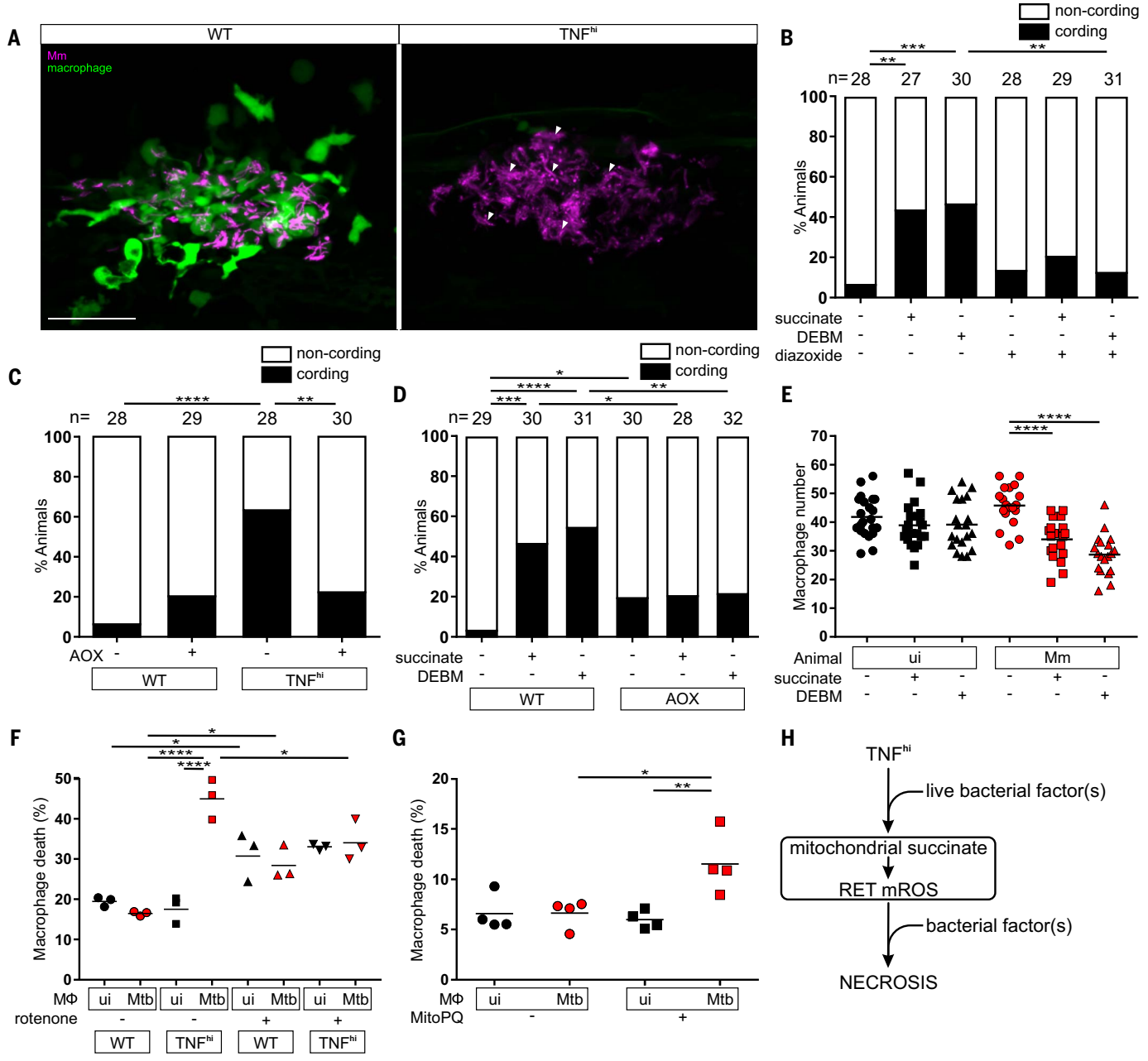

Fig. 6. TNF-mediated increased glutamine cellular uptake in mycobacterium-infected macrophages increases succinate oxidation, mROS, and necrosis. (**A**) Representative pseudocolored confocal images of 5-dpi granulomas in wild-type or TNF^{hi} larvae with YFP-expressing macrophages (green) infected with tdTomato-expressing *Mm* (magenta). Arrowheads, extracellular cording bacteria. Scale bar, 50 μm. (**B**) Bacterial cording in wild-type larvae 5 days after infection with *Mm*, treated with vehicle, or succinate or DEBM alone or in combination with diazoxide; $^{**}P < 0.01$, $^{***}P < 0.001$ (Fisher's exact test). (**C**) Bacterial cording 5 days after infection with *Mm* in wild-type and TNF^{hi} larvae and wild-type and TNF^{hi} larvae expressing AOX; $^{**}P < 0.01$, $^{****}P < 0.0001$ (Fisher's exact test). (**D**) Bacterial cording 5 days after infection with wild-type or AOX-expressing larvae infected with *Mm* and treated with succinate, DEBM, or vehicle; $^{*}P < 0.05$, $^{**}P < 0.01$, $^{***}P < 0.001$, $^{****}P < 0.0001$ (Fisher's exact test). (**E**) Number of trunk macrophages in *Mm*-infected larvae and mock-injected (ui) larvae 1 day after infection. Horizontal bars denote means; $^{****}P < 0.0001$ (one-way ANOVA with Dunn's post-test). (**F** and **G**) Percentage of dead THP-1 macrophages 5 hours after addition of TNF, treated with rotenone or vehicle starting 1 hour before TNF addition (F) or MitoParaquat (MitoPQ) or vehicle for 5 hours (G). Black and red symbols represent uninfected (ui) and *Mtb*-infected macrophages, respectively, within the same treatment well. Horizontal bars denote means; $^{*}P < 0.05$, $^{**}P < 0.01$, $^{****}P < 0.0001$ (one-way ANOVA with Tukey's post-test). (**H**) Schematic diagram showing the role of TNF, mROS, and mycobacterial factor(s) in TNF-mediated necrosis of mycobacterium-infected macrophages. Data are representative of two independent experiments [(C), (D), (E), and (G)] or a single experiment [(B) and (F)].

Downloaded from https://www.science.org at University Van Amsterdam on April 13, 2025

production, as disrupting the ETC with diazoxide reduced cording (Fig. 6B). Moreover, bypassing the ETC by AOX expression—which decreased TNF-induced mROS (Fig. 2E)—inhibited TNF-mediated macrophage necrosis (Fig. 6C) as well as succinate- and DEBM-induced necrosis in wild-type animals (Fig. 6D). Thus, TNF plays no further role in macrophage necrosis beyond increasing mitochondrial succinate.

To determine whether mycobacteria were required for necrosis downstream of mROS induction, we examined whether diethyl succinate and DEBM could also kill uninfected macrophages by enumerating macrophages in infected and uninfected animals (*5*). Diethyl succinate and DEBM reduced macrophage numbers only in the infected animals; this finding suggests that unlike TNF, mycobacteria are required downstream of mROS to induce necrosis (Fig. 6E and fig. S2).

Similar results were observed in human macrophages derived from the monocytic cell line THP-1. We previously showed that TNF induces necrosis in *Mtb*-infected THP-1 cells through the same interorganellar pathway downstream of mROS as in *Mm*-infected zebrafish (fig. S2) (*6*). We used rotenone to confirm that RET was responsible for mROS induction in these cells. In the absence of TNF, rotenone increased death of both infected and uninfected cells, as expected from the oxidative stress it induces, but we found a specific reduction of TNF-induced death of infected macrophages (Fig. 6F). Next, to test our findings from zebrafish concerning the role of TNF, mROS, and mycobacteria, we treated *Mtb*-infected THP-1 cells with MitoParaquat (MitoPQ), a mitochondria-targeted compound that produces superoxide through redox cycling at the complex I flavin site (table S1). MitoPQ increased necrosis in the absence of TNF but only in infected macrophages (Fig. 6G and fig. S2). This confirmed that TNF has no further role in the necrosis pathway beyond inducing mROS, whereas mycobacteria are required downstream of mROS induction. One or more mycobacterial factors shared between *Mm* and *Mtb* operate at two distinct points in this pathway: first to enable TNF-mediated mROS by activating cellular glutamine uptake and increasing mitochondrial succinate to produce complex II–mediated RET-ROS, and then to promote the necrosis of macrophages experiencing this mROS (Fig. 6H).

The mROS pathway reveals host-targeting drugs for TB

We previously showed that blocking mROS using scavengers such as *N*-acetylcysteine inhibited TNF-induced macrophage necrosis and restored resistance (*5*). Four of the compounds used here to inhibit mROS, and thus to delineate the mechanism of mROS production, are approved oral drugs or are under investigation for other conditions. We therefore assessed whether these drugs also inhibited macrophage necrosis (fig. S5). These included diazoxide, a disruptor of electron transport that is approved for hyperinsulinemic hypoglycemia; perhexiline, a mitochondrial carnitine palmitoyltransferase-1 inhibitor that is approved for angina; telaglenastat, a GLS1 inhibitor that is in clinical trials for cancer; and DM-malonate, the complex II inhibitor that has been shown to prevent ischemia-reperfusion injury in models of heart attack (fig. S5 and table S1) (*28*). All four inhibited TNF-mediated macrophage necrosis in zebrafish (Fig. 7, A to E). We then asked whether metformin, a widely used antidiabetic drug that inhibits complex I (fig. S5 and table S1) (*29*), could be a potential host-targeting drug to prevent TNF-induced pathogenic macrophage necrosis in TB. Metformin inhibited TNF-elicited mROS in *Mm*-infected larvae, as did its more hydrophobic derivative, phenformin (Fig. 7F). Metformin also inhibited TNF-mediated necrosis of *Mm*-infected macrophages (Fig. 7G). Moreover, it also inhibited *Mm*-infected macrophage necrosis resulting from increased mitochondrial succinate (Fig. 7H). Thus, although metformin has pleiotropic effects and is a relatively weak complex I inhibitor (*29*), it specifically inhibits TNF-mediated necrosis by blocking RET-generated mROS at complex I. Finally, metformin inhibited mROS in the infected macrophages of *Mtb*-infected zebrafish (Fig. 7I) and inhibited necrosis of *Mtb*-infected THP-1 cells (Fig. 7J), thereby confirming that its inhibitory activity was relevant in the context of *Mtb* infection.

Discussion

Although long thought to be an in vitro artifact, moderate levels of RET and resultant increases in mROS have important homeostatic roles in cell differentiation and oxygen sensing (*13*). However, excess RET has pathological roles in ischemia-reperfusion injury of the heart and brain (*18*, *30*). During ischemia, rewiring of the Krebs cycle reduces fumarate concentrations, leading to succinate accumulation (*18*). During the reperfusion phase, rapid oxidation of the accumulated succinate triggers RET and mROS, which causes tissue necrosis leading to irreparable organ damage (*18*, *30*). The TNF-mediated necrosis pathway described here has two important differences. First, the source of the succinate is different; second, in ischemia-reperfusion injury, the mROS alone appear sufficient to drive necrosis, whereas a second "hit" in the form of one or more bacterial determinants is required in our TNF-induced macrophage necrosis pathway. Perhaps the inflammatory milieu generated during ischemia generates the additional signal(s) that combine with mROS to cause necrosis.

Work using cultured macrophages has shown that succinate is responsible for generating proinflammatory responses to lipopolysaccharide (LPS), a key virulence determinant of Gram-negative bacteria (*19*). LPS causes macrophages to switch to aerobic glycolysis while generating succinate from enhanced glutaminolysis by an undescribed means. Succinate induces mROS, likely through RET, and these mROS drive proinflammatory cytokines via hypoxia-inducible factor–1α stabilization (*19*, *31*). This sequence contrasts with the pathway described here, where TNF is upstream, not downstream, of mROS and TNF is not among the cytokines induced by LPS and succinate. Thus, distinct pathogenic determinants specific to Gram-negative bacteria and mycobacteria—a cell wall constituent versus a product of live mycobacteria—channel mROS to produce discrete cellular responses.

We were particularly interested in pursuing this TNF-mediated necrosis pathway because of its clinical implications. Currently, tuberculous meningitis is treated with adjunctive corticosteroids, which are broadly immunosuppressive and have multiple additional serious adverse effects. Our prior studies on the TNF-mediated necrosis pathway identified several pathway-specific drugs that inhibit macrophage necrosis without being broadly anti-inflammatory, all with a decades-long history of use in humans for other conditions (*5*, *6*). This work now identifies additional drugs, including the widely used oral antidiabetic drug metformin. Metformin readily crosses the blood-brain barrier, resulting in high brain and cerebrospinal fluid concentrations (table S1) (*32*). This highlights its potential therapeutic utility in tuberculous meningitis. Metformin was reported to ameliorate *Mtb* infection in mice via diverse mechanisms, including broadly acting anti-inflammatory effects, and to enhance the efficacy of antitubercular antibiotics in one but not another study, leading to an ongoing trial as an adjunctive agent for lung TB (*33*–*36*). Adjunctive corticosteroid treatment has been suggested to reduce inflammation and bacterial burdens in lung TB, the most common, contagious form that sustains the global disease burden (*37*, *38*). It will be interesting to see whether metformin particularly benefits individuals with the high-*LTA4H* genotype. Moreover, given the association of TNF with necrotic lung granulomas (*11*), metformin may increase resolution of necrotic lesions.

Materials and methods

Zebrafish husbandry and infections

Zebrafish husbandry and experiments were conducted in compliance with guidelines from the UK Home Office using protocols approved

Downloaded from https://www.science.org at University Van Amsterdam on April 13, 2025

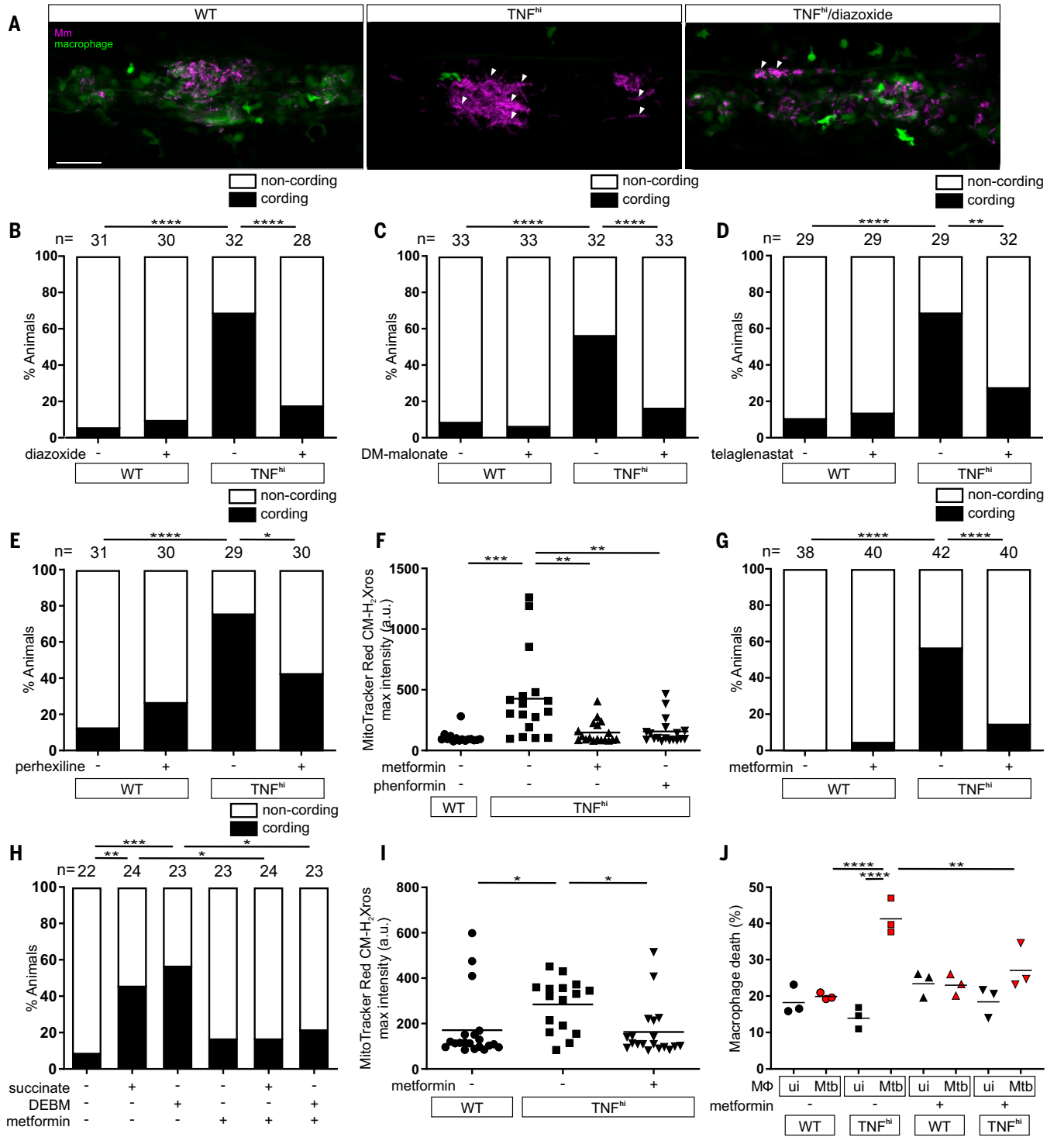

Fig. 7. Currently available drugs can intercept TNF-induced mROS production and inhibit necrosis of mycobacterium-infected macrophages. (**A**) Representative pseudocolored confocal images of 5-dpi granulomas in larvae with YFP-stained macrophages (green) that are wild-type or TNF^{hi} treated with diazoxide or vehicle, infected with red fluorescent *Mm* (magenta). Arrowheads, extracellular cording bacteria. Scale bar, 50 μm. (**B** to **E**) Bacterial cording in wild-type or TNF^{hi} larvae 5 days after infection with *Mm*, treated with vehicle or diazoxide (B), DM-malonate (C), telaglenastat (D), or perhexiline (E). *P < 0.05, **P < 0.01, ****P < 0.0001 (Fisher's exact test). (**F**) Quantification of mROS in wild-type or TNF^{hi} larvae 1 day after infection with *Mm*, treated with metformin, phenformin, or vehicle. Horizontal bars denote means; **P < 0.01, ***P < 0.001 (one-way ANOVA with Tukey's post-test). (**G**) Bacterial cording in wild-type or TNF^{hi} larvae 5 days after infection with *Mm*, treated with metformin or vehicle. ****P < 0.0001 (Fisher's exact test). (**H**) Bacterial cording in wild-type larvae 5 days after infection with *Mm*, treated with vehicle or with succinate or DEBM alone or in combination with metformin. *P < 0.05, **P < 0.01, ***P < 0.001 (Fisher's exact test). (**I**) Quantification of mROS in wild-type or TNF^{hi} 1 day after infection with *Mtb*, treated with metformin or vehicle. Horizontal bars denote means; *P < 0.05 (one-way ANOVA with Tukey's post-test). (**J**) Percentage

Downloaded from https://www.science.org at University Van Amsterdam on April 13, 2025

of dead THP-1 macrophages at 5 hours after addition of TNF, treated with metformin or vehicle starting 1 hour before TNF addition. Black and red symbols represent uninfected (ui) and *Mtb*-infected macrophages, respectively, within the same treatment well. Horizontal bars denote means; $^{**}P < 0.01$, $^{****}P < 0.0001$ (one-way ANOVA with Tukey's post-test). Data are representative of two independent experiments [(B) to (G) and (I)] or a single experiment [(H) and (J)].

by the Animal Welfare and Ethical Review Body of the University of Cambridge. Zebrafish AB wild-type strain (Zebrafish International Resource Center) (ZFIN ID: ZDB-GENO-960809-7) and the transgenic line *Tg(mpeg1:YFP)*^{w200} (with yellow fluorescent macrophages) (ZFIN ID: ZDB-FISH-150901-6828) (*6*) in the AB background were used. All zebrafish lines were maintained in buffered reverse osmotic water systems as described (*6*). Zebrafish embryos were housed at 28.5°C in fish water from collection to 1 day post-fertilization (dpf) and in E2 Embryo Medium diluted to 0.5× (E2/2) supplemented with 0.003% 1-phenyl-2-thiourea (PTU) (Sigma) from 1 dpf to prevent pigmentation (*6*). Larvae (of undetermined sex given the early developmental stages used) were anesthetized, infected at 2 dpf via caudal vein (CV) injection for all assays, and randomly allotted to the different experimental conditions as described (*6*, *39*). Sample size was determined based on previous similar experiments or on pilot experiments.

Bacterial strains

Mm M strain (ATCC #BAA-535) and *Mtb* H37Rv strain, mc^{2}6206 Δ*leuD* Δ*panCD* (*40*) expressing tdTomato, mWasabi, or EBFP2 were grown as described (*39*, *41*). For experiments to assay bacterial cording and number of macrophages in the trunk of the animal, zebrafish larvae were infected with 150 to 200 tdTomato-expressing *Mm*. To assess mROS, larvae were infected with 90 to 120 EBFP2-expressing or 84 mWasabi-expressing *Mm*, 80 to 100 EBFP2-expressing *Mtb*, or injected with 336 heat-killed mWasabi-expressing *Mm* (heat-killed by incubation at 80°C for 20 min). To assess succinate levels, larvae were infected with 200 to 300 tdTomato-expressing *Mm*.

TNF and drug administration to zebrafish larvae

TNF^{hi} animals were created by injecting recombinant zebrafish soluble TNF (*42*) as described (*4*). To assess drug treatment in infected animals, equivalently infected sibling larvae were mixed in a petri dish and held at 28.5°C before random allocation to the drug-treated or control groups; 0.5% DMSO (Sigma) was used as the control (vehicle). Drugs dissolved in DMSO or water were kept in small aliquots at −20°C before administration to 1-dpi larvae by adding them to the water (E2/2 medium). Doses used in this work were based on previous studies or pilot experiments, using the minimum effective concentration without deleterious or toxic effects on larvae for the duration of the experiment (see table S2). FCCP [carbonyl cyanide-4-(trifluoromethoxy)phenylhydrazone] (50 nM; Cambridge Bioscience) was administered 1.5 hours before MitoTracker Red CM-H_2-Xros injection. TTFA (1 μM; Cambridge Bioscience), atpenin A5 (2.5 nM; Insight Biotechnology), diethyl succinate (500 nM; reagent plus 99%, Sigma), and DEBM (diethyl butyl malonate) (1 μM; Sigma) were administered 2 hours before MitoTracker Red CM-H_2-Xros injection. DM-glutamate (dimethyl glutamate) (60 μM; Cambridge Bioscience) was administered 3 hours before MitoTracker Red CM-H_2-Xros Injection. DNP (2.4-dinitrophenol) (100 nM; Agilent Technologies) was administered 3.5 hours before MitoTracker Red CM-H_2-Xros injection. Rotenone (6.25 nM; Sigma), piericidin A (50 nM; Stratech Scientific), strobilurin B (100 nM; Insight Biotechnology), metformin (20 μM; VWR International), phenformin (20 μM; Sigma), nigericin (5 μM; Sigma), diazoxide (50 nM; Cambridge Bioscience), UK5099 (10 μM; Cambridge Bioscience), and M-pyruvate (methyl pyruvate) (50 nM; Fisher Scientific) were administered 4 hours before MitoTracker Red CM-H_2-Xros injection. DM-malonate (10 μM; Sigma), perhexiline (10 μM; Stratech Scientific), 4-BrCA (4-bromocrotonic acid) (10 μM; Insight Biotechnology), GPNA (10 μM; Cambridge Bioscience), BPTES (5 μM; Cambridge Bioscience), telaglenastat (5 μM; Cambridge Bioscience), and R-162 (1 μM; Cambridge Bioscience) were administered 5 hours before MitoTracker Red CM-H_2-Xros injection. In experiments to assess cording, perhexiline was removed 5 hours after TNF administration, diethyl succinate and DEBM were administered for 10 hours and then removed, and metformin, phenformin, DM-malonate, diazoxide, and telaglenastat were added at 1 dpi and removed at 2 dpi. After drug removal, the larvae were maintained in fresh E2/2 medium for the rest of the experiment. In experiments to assess macrophage numbers, diethyl succinate and DEBM were administered at 2 dpf/1 dpi for 24 hours until macrophage number was assessed at 3 dpf/2 dpi. For experiments quantifying mitochondrial ROS production, drugs were added before MitoTracker Red CM-H_2-Xros injection as indicated above and maintained during imaging.

Synthetic mRNA synthesis and microinjection

The ORF sequence of the alternative oxidase (AOX) from *Ciona intestinalis* was obtained by PCR using as a template the plasmid MAC_C_AOX (Addgene plasmid #111661). The T7 promoter (5′-TAATACGACTCACTATAGG-3′) followed by the zebrafish Kozak sequence 5′-GCCGCCACC-3′ were inserted before the start codon by PCR. mRNA was synthesized using the mMessage mMachine kit (Ambion) and the polyA Tailing kit (Ambion). Approximately 2 to 4 nl of injection solution (*4*) containing AOX mRNA (200 μg/ml) was injected into the yolks of embryos at the one- to two-cell stage.

Morpholino-mediated knockdown of RIP3 and PGAM5

RIP3 e2/i2 splice-blocking (5′-TTTTAGAAATCACCTTGGCATCCAG-3′) and PGAM5 translation-blocking morpholino (5′-AGCGCCCTCCGAAAAGACATGCTTC-3′) (Gene Tools) were diluted to 0.15 mM in injection solution (*4*). Approximately 2 to 4 nl was injected into the yolks of embryos at the one- to two-cell stage.

Heart rate assessment of zebrafish larvae

AOX-expressing 2-dpf larvae were treated with different concentrations of KCN for an hour. Heart rate (beats per minute) was assessed as a readout of cyanide poisoning of complex IV of the electron transport chain (*43*) in the absence of anesthetic using a dissecting microscope.

Zebrafish larva microscopy

Fluorescence microscopy was performed as described (*39*). Mycobacterial cording and macrophage numbers were assessed in the trunk of the larvae using a Nikon Eclipse E600 upright microscope fitted with Nikon Plan Fluor 10× 0.3 NA and Nikon Plan Fluor 20× 0.5 NA objectives. For laser scanning confocal microscopy, anesthetized larvae were embedded in low-melting-point agarose as described (*6*). A Nikon A1R confocal microscope with a Plan Apo 20× 0.75 NA objective was used to generate 35- to 40-mm *z*-stacks consisting of 0.3- to 2-mm optical sections. The galvano scanner was used for all static imaging and for time-lapse imaging of the caudal hematopoietic tissue (CHT, area located between the cloaca and the beginning of the caudal fin). Images were acquired with NIS Elements (Nikon). A heating chamber (Oko-labs) adapted to the microscope was used to maintain temperature at 28.5°C during imaging. Confocal images are pseudocolored to facilitate visualization.

Mitochondrial ROS quantification assay in zebrafish larvae

Mitochondrial ROS production was assayed by fluorescence intensity of MitoTracker Red CM-H_2-Xros, a cell-permeable fluorogenic probe for ROS, which is targeted to the mitochondrion and produces red fluorescence upon oxidation by diverse ROS (Fisher Scientific) (*5*, *6*). *Tg (mpeg1:YFP)*^{w200} larvae were infected at 2 dpf.

Downloaded from https://www.science.org at University Van Amsterdam on April 13, 2025

For all experiments where TNF^{hi} animals were used, larvae were microinjected at 1 dpi via CV with phosphate-buffered saline (PBS) containing TNF and 50 mM MitoTracker Red CM-H_2-Xros or PBS containing vehicle for TNF and MitoTracker Red CM-H_2-Xros (*6*). For experiments where mROS production was quantified in mycobacterium-infected versus uninfected macrophages, 100 mM MitoTracker Red CM-H_2-Xros was used instead to increase sensitivity of the probe. After administration of MitoTracker Red CM-H_2-Xros (in combination with TNF or alone), larvae were prepared for confocal imaging and maintained at 28.5°C within a heated incubation chamber attached to the confocal microscope. Images of the CHT of each larva were taken starting 30 to 60 min after MitoTracker Red CM-H_2-Xros administration. Mitochondrial ROS production was quantified using maximum projection images as MitoTracker Red CM-H_2-Xros maximum fluorescence intensity per macrophage using NIS-Elements. When not otherwise stated in the figure legend, the mean of maximum MitoTracker Red CM-H_2-Xros fluorescence was quantified only in *Mm*- or *Mtb*-infected macrophages.

Succinate quantification by liquid chromatography–mass spectrometry

Three to six pools of 20 1-dpi larvae per condition per experiment were collected and flash-frozen 30 min after TNF injection, with the time set after injecting 75% of the larvae for each experimental group. Each pool was homogenized in 300 μl of extraction buffer and succinate was quantified as described (*44*). The means and pooled standard deviations of independent experiments were calculated and compared using one-way analysis of variance (ANOVA) with Tukey's post hoc multiple comparisons test.

Quantification of THP-1 cell necrosis

THP-1 cells (ATCC TIB-202) were differentiated into macrophages and infected with single-cell suspensions of mCherry- or tdTomato-expressing *Mtb* mc^{2}6206 Δ*leuD* Δ*panCD* as described (*6*). In THP-1 experiments with added TNF, 1-dpi cells were pre-incubated with 10 nM rotenone, 1 mM metformin, or 0.1% DMSO vehicle control for 1 hour. Human recombinant TNF (Sigma) in a solution of 5% trehalose/PBS (Sigma) was then added to treatment wells as described (*6*). In the experiment with 5 μM mitoparaquat, drug or 0.1% DMSO vehicle control was added 1 day after *Mtb* infection and images acquired after 5 hours of incubation. SYTOX Green Nucleic Acid Stain (Life Technologies) was added to culture medium 30 min before image acquisition. Macrophages were imaged using a Nikon Ti-E inverted microscope fitted with a 20× objective (Nikon, CFI S Plan Fluor 0.45 NA) and two to five arbitrary images per well acquired with NIS Elements (Nikon). Cell necrosis was quantified as described (*6*).

Statistical analysis

The following statistical analyses were performed using Prism 7 (GraphPad): two-way ANOVA or one-way ANOVA with Dunn's or Tukey's post-test and Fisher's exact test. Error bars denote SEM. Post-test P values were defined as follows: $^*P < 0.05$, $^{**}P < 0.01$, $^{***}P < 0.001$, $^{****}P < 0.0001$ (not significant, $P > 0.05$). Where the n value is given in a figure and not represented graphically in the figure, n represents the number of zebrafish used for each experimental group.

Software used

The following software was used: NIS-Elements for image acquisition in wide-field and confocal microscopy, ImageJ (https://fiji.sc/) for image analysis of macrophage death, GraphPad Prism 7.0 (GraphPad Software) for data graphing and statistical analyses, and CorelDRAW (CorelDRAW Graphics Suite x5) for figure preparation.

REFERENCES AND NOTES

1. J. Keane *et al*., Tuberculosis associated with infliximab, a tumor necrosis factor α-neutralizing agent. *N. Engl. J. Med.* **345**, 1098–1104 (2001). doi: 10.1056/NEJMoa011110; pmid: 11596589
2. M. A. Behr, P. H. Edelstein, L. Ramakrishnan, Is *Mycobacterium tuberculosis* infection life long? *BMJ* **367**, l5770 (2019). doi: 10.1136/bmj.l5770; pmid: 31649096
3. L. J. Whitworth *et al*., Elevated cerebrospinal fluid cytokine levels in tuberculous meningitis predict survival in response to dexamethasone. *Proc. Natl. Acad. Sci. U.S.A.* **118**, e2024852118 (2021). doi: 10.1073/pnas.2024852118; pmid: 33658385
4. D. M. Tobin *et al*., Host genotype-specific therapies can optimize the inflammatory response to mycobacterial infections. *Cell* **148**, 434–446 (2012). doi: 10.1016/j.cell.2011.12.023; pmid: 22304914
5. F. J. Roca, L. Ramakrishnan, TNF dually mediates resistance and susceptibility to mycobacteria via mitochondrial reactive oxygen species. *Cell* **153**, 521–534 (2013). doi: 10.1016/j.cell.2013.03.022; pmid: 23582643
6. F. J. Roca, L. J. Whitworth, S. Redmond, A. A. Jones, L. Ramakrishnan, TNF Induces Pathogenic Programmed Macrophage Necrosis in Tuberculosis through a Mitochondrial-Lysosomal-Endoplasmic Reticulum Circuit. *Cell* **178**, 1344–1361.e11 (2019). doi: 10.1016/j.cell.2019.08.004; pmid: 31474371
7. C. J. Cambier, S. Falkow, L. Ramakrishnan, Host evasion and exploitation schemes of Mycobacterium tuberculosis. *Cell* **159**, 1497–1509 (2014). doi: 10.1016/j.cell.2014.11.024; pmid: 25525872
8. H. Clay, H. E. Volkman, L. Ramakrishnan, Tumor necrosis factor signaling mediates resistance to mycobacteria by inhibiting bacterial growth and macrophage death. *Immunity* **29**, 283–294 (2008). doi: 10.1016/j.immuni.2008.06.011; pmid: 18691913
9. D. M. Tobin *et al*., The lta4h locus modulates susceptibility to mycobacterial infection in zebrafish and humans. *Cell* **140**, 717–730 (2010). doi: 10.1016/j.cell.2010.02.013; pmid: 20211140
10. L. Whitworth *et al*., A Bayesian analysis of the association between *Leukotriene A4 Hydrolase* genotype and survival in tuberculous meningitis. *eLife* **10**, e61722 (2021). doi: 10.7554/eLife.61722; pmid: 33416499
11. M. J. Marakalala *et al*., Inflammatory signaling in human tuberculosis granulomas is spatially organized. *Nat. Med.* **22**, 531–538 (2016). doi: 10.1038/nm.4073; pmid: 27043495
12. M. P. Murphy, How mitochondria produce reactive oxygen species. *Biochem. J.* **417**, 1–13 (2009). doi: 10.1042/BJ20081386; pmid: 19061483
13. F. Scialò, D. J. Fernández-Ayala, A. Sanz, Role of Mitochondrial Reverse Electron Transport in ROS Signaling: Potential Roles in Health and Disease. *Front. Physiol.* **8**, 428 (2017). doi: 10.3389/fphys.2017.00428; pmid: 28701960
14. R. Fato *et al*., Differential effects of mitochondrial Complex I inhibitors on production of reactive oxygen species. *Biochim. Biophys. Acta* **1787**, 384–392 (2009). doi: 10.1016/j.bbabio.2008.11.003; pmid: 19059197
15. E. L. Robb *et al*., Control of mitochondrial superoxide production by reverse electron transport at complex I. *J. Biol. Chem.* **293**, 9869–9879 (2018). doi: 10.1074/jbc.RA118.003647; pmid: 29743240
16. H. Nůsková, M. Vrbacký, Z. Drahota, J. Houštěk, Cyanide inhibition and pyruvate-induced recovery of cytochrome c oxidase. *J. Bioenerg. Biomembr.* **42**, 395–403 (2010). doi: 10.1007/s10863-010-9307-6; pmid: 20725851
17. N. Burger *et al*., A sensitive mass spectrometric assay for mitochondrial CoQ pool redox state in vivo. *Free Radic. Biol. Med.* **147**, 37–47 (2020). doi: 10.1016/j.freeradbiomed.2019.11.028; pmid: 31811922
18. E. T. Chouchani *et al*., Ischaemic accumulation of succinate controls reperfusion injury through mitochondrial ROS. *Nature* **515**, 431–435 (2014). doi: 10.1038/nature13909; pmid: 25383517
19. E. L. Mills *et al*., Succinate Dehydrogenase Supports Metabolic Repurposing of Mitochondria to Drive Inflammatory Macrophages. *Cell* **167**, 457–470.e13 (2016). doi: 10.1016/j.cell.2016.08.064; pmid: 27667687
20. D. W. Zhang *et al*., RIP3, an energy metabolism regulator that switches TNF-induced cell death from apoptosis to necrosis. *Science* **325**, 332–336 (2009). doi: 10.1126/science.1172308; pmid: 19498109
21. V. Goossens, G. Stangé, K. Moens, D. Pipeleers, J. Grooten, Regulation of tumor necrosis factor-induced, mitochondria- and reactive oxygen species-dependent cell death by the electron flux through the electron transport chain complex I. *Antioxid. Redox Signal.* **1**, 285–295 (1999). doi: 10.1089/ars.1999.1.3-285; pmid: 11229440
22. www.proteinatlas.org/.
23. A. Bröer, F. Rahimi, S. Bröer, Deletion of Amino Acid Transporter ASCT2 (SLC1A5) Reveals an Essential Role for Transporters SNAT1 (SLC38A1) and SNAT2 (SLC38A2) to Sustain Glutaminolysis in Cancer Cells. *J. Biol. Chem.* **291**, 13194–13205 (2016). doi: 10.1074/jbc.M115.700534; pmid: 27129276
24. www.sanger.ac.uk/tool/basicz/.
25. C. Q. Zhong *et al*., Quantitative phosphoproteomic analysis of RIP3-dependent protein phosphorylation in the course of TNF-induced necroptosis. *Proteomics* **14**, 713–724 (2014). doi: 10.1002/pmic.201300326; pmid: 24453211
26. A. Stepanova, Y. Shurubor, F. Valsecchi, G. Manfredi, A. Galkin, Differential susceptibility of mitochondrial complex II to inhibition by oxaloacetate in brain and heart. *Biochim. Biophys. Acta* **1857**, 1561–1568 (2016). doi: 10.1016/j.bbabio.2016.06.002; pmid: 27287543
27. Z. Wang, H. Jiang, S. Chen, F. Du, X. Wang, The mitochondrial phosphatase PGAM5 functions at the convergence point of multiple necrotic death pathways. *Cell* **148**, 228–243 (2012). doi: 10.1016/j.cell.2011.11.030; pmid: 22265414
28. H. A. Prag *et al*., Ester Prodrugs of Malonate with Enhanced Intracellular Delivery Protect Against Cardiac Ischemia-Reperfusion Injury In Vivo. *Cardiovasc. Drugs Ther.* **36**, 1–13 (2022). doi: 10.1007/s10557-020-07033-6; pmid: 32648168
29. G. Vial, D. Detaille, B. Guigas, Role of Mitochondria in the Mechanism(s) of Action of Metformin. *Front. Endocrinol.* **10**, 294 (2019). doi: 10.3389/fendo.2019.00294; pmid: 31133988
30. A. Stepanova *et al*., Reverse electron transfer results in a loss of flavin from mitochondrial complex I: Potential mechanism for brain ischemia reperfusion injury. *J. Cereb. Blood Flow Metab.* **37**, 3649–3658 (2017). doi: 10.1177/0271678X17730242; pmid: 28914132
31. G. M. Tannahill *et al*., Succinate is an inflammatory signal that induces IL-1β through HIF-1α. *Nature* **496**, 238–242 (2013). doi: 10.1038/nature11986; pmid: 23535595
32. K. Łabuzek *et al*., Quantification of metformin by the HPLC method in brain regions, cerebrospinal fluid and plasma of rats treated with lipopolysaccharide. *Pharmacol. Rep.* **62**, 956–965 (2010). doi: 10.1016/S1734-1140(10)70357-1; pmid: 21098880

Downloaded from https://www.science.org at University Van Amsterdam on April 13, 2025

33. A. Singhal *et al*., Metformin as adjunct antituberculosis therapy. *Sci. Transl. Med.* **6**, 263ra159 (2014). doi: 10.1126/scitranslmed.3009885; pmid: 25411472
34. L. Tsenova, A. Singhal, Effects of host-directed therapies on the pathology of tuberculosis. *J. Pathol.* **250**, 636–646 (2020). doi: 10.1002/path.5407; pmid: 32108337
35. C. Padmapriyadarsini *et al*., Evaluation of metformin in combination with rifampicin containing antituberculosis therapy in patients with new, smear-positive pulmonary tuberculosis (METRIF): Study protocol for a randomised clinical trial. *BMJ Open* **9**, e024363 (2019). doi: 10.1136/bmjopen-2018-024363; pmid: 30826761
36. N. K. Dutta, M. L. Pinn, P. C. Karakousis, Metformin Adjunctive Therapy Does Not Improve the Sterilizing Activity of the First-Line Antitubercular Regimen in Mice. *Antimicrob. Agents Chemother.* **61**, 00652-17 (2017). https://doi.org/10.1128/aac.00652-17
37. P. Muthuswamy, T. C. Hu, B. Carasso, M. Antonio, N. Dandamudi, Prednisone as adjunctive therapy in the management of pulmonary tuberculosis. Report of 12 cases and review of the literature. *Chest* **107**, 1621–1630 (1995). doi: 10.1378/chest.107.6.1621; pmid: 7781357
38. R. A. Smego, N. Ahmed, A systematic review of the adjunctive use of systemic corticosteroids for pulmonary tuberculosis. *Int. J. Tuberc. Lung Dis.* **7**, 208–213 (2003). pmid: 12661833
39. K. Takaki, J. M. Davis, K. Winglee, L. Ramakrishnan, Evaluation of the pathogenesis and treatment of Mycobacterium marinum infection in zebrafish. *Nat. Protoc.* **8**, 1114–1124 (2013). doi: 10.1038/nprot.2013.068; pmid: 23680983
40. J. M. Mouton *et al*., Comprehensive Characterization of the Attenuated Double Auxotroph *Mycobacterium tuberculosisΔleuDΔpanCD* as an Alternative to H37Rv. *Front. Microbiol.* **10**, 1922 (2019). doi: 10.3389/fmicb.2019.01922; pmid: 31481950
41. M. M. Osman *et al*., The C terminus of the mycobacterium ESX-1 secretion system substrate ESAT-6 is required for phagosomal membrane damage and virulence. *Proc. Natl. Acad. Sci. U.S.A.* **119**, e2122161119 (2022). doi: 10.1073/pnas.2122161119; pmid: 35271388
42. F. J. Roca *et al*., Evolution of the inflammatory response in vertebrates: Fish TNF-α is a powerful activator of endothelial cells but hardly activates phagocytes. *J. Immunol.* **181**, 5071–5081 (2008). doi: 10.4049/jimmunol.181.7.5071; pmid: 18802111
43. A. K. Nath *et al*., Chemical and metabolomic screens identify novel biomarkers and antidotes for cyanide exposure. *FASEB J.* **27**, 1928–1938 (2013). doi: 10.1096/fj.12-225037; pmid: 23345455
44. H. A. Prag *et al*., Mechanism of succinate efflux upon reperfusion of the ischaemic heart. *Cardiovasc. Res.* **117**, 1188–1201 (2021). doi: 10.1093/cvr/cvaa148; pmid: 32766828

ACKNOWLEDGMENTS

We thank J. Walker for sharing his knowledge and insights, advice, critical appraisal of the work through the years, and critical review of the paper; P. Edelstein for help and advice on statistical analysis and critical review of the paper; D. Tobin and E. Kunji for critical review of the paper; N. Burger for discussion on mass spectrometry assays and results; J. Baeck for toxicity testing of several of the compounds used and preliminary assessments of the effects of some; K. Takaki, J. Fan, and B. Lyu for help with experiments to quantify succinate; N. Goodwin, R. Foster, and the University of Cambridge aquatics facility staff for zebrafish husbandry; and the LMB's media service for preparation of bacterial and tissue culture reagents. **Funding:** Supported by Wellcome Trust Principal Research Fellowship 223103/Z/21/Z and NIH MERIT award R37 AI054503 (L.R.), Medical Research Council UK grant MC_U105663142 and Wellcome Trust Investigator award 110159/A/15/Z (M.P.M.), and MCIN and "ESF Investing in your Future" Fellowship RYC2019-027799-I/AEI/10.13039/501100011033 (F.J.R.). **Author contributions:** F.J.R. and L.R. designed the project. F.J.R., L.J.W., and H.A.P. performed experiments. F.J.R., L.J.W., H.A.P., L.R., and M.P.M. designed experiments and analyzed and interpreted data. F.J.R. and L.R. wrote the paper. All authors edited the paper with input from the other authors. **Competing interests:** The authors declare that they have no competing interests. **Data and materials availability:** All data are available in the main text or the supplementary materials. **License information:** To facilitate open access, the authors have applied a CC BY public copyright license to any Author Accepted Manuscript version arising from this submission. This work is licensed under a Creative Commons Attribution 4.0 International License.

SUPPLEMENTARY MATERIALS

science.org/doi/10.1126/science.abh2841
Figs. S1 to S5
Tables S1 and S2
References (*45*–*64*)
Data S1
MDAR Reproducibility Checklist

View/request a protocol for this paper from *Bio-protocol*.

Submitted 26 February 2021; resubmitted 24 November 2021
Accepted 9 May 2022
10.1126/science.abh2841

Downloaded from https://www.science.org at University Van Amsterdam on April 13, 2025